



## Article

# Generational Diet-Induced Obesity Remodels the Omental Adipose Proteome in Female Mice

Naviya Schuster-Little <sup>1,2</sup>, Morgan McCabe <sup>3</sup>, Kayla Nenninger <sup>3</sup>, Reihaneh Safavi-Sohi <sup>3,4,5</sup>,  
Rebecca J. Whelan <sup>1,2,†</sup> and Tyvette S. Hilliard <sup>3,4,\*,†</sup>

<sup>1</sup> Department of Chemistry, University of Kansas, Lawrence, KS 66045, USA; naviya@ku.edu (N.S.-L.); rwhelan1@ku.edu (R.J.W.)

<sup>2</sup> Ralph N. Adams Institute for Bioanalytical Chemistry, University of Kansas, Lawrence, KS 66047, USA

<sup>3</sup> Department of Chemistry and Biochemistry, University of Notre Dame, Notre Dame, IN 46556, USA; mmccabe7@alumni.nd.edu (M.M.); knenning@alumni.nd.edu (K.N.); rsafavis@nd.edu (R.S.-S.)

<sup>4</sup> Harper Cancer Research Institute, University of Notre Dame, Notre Dame, IN 46617, USA

<sup>5</sup> Department of Chemistry and Biochemistry, Seton Hall University, South Orange, NJ 07079, USA

\* Correspondence: thilliar@nd.edu

† These authors share senior authorship.

**Abstract:** Obesity, a complex condition that involves genetic, environmental, and behavioral factors, is a non-infectious pandemic that affects over 650 million adults worldwide with a rapidly growing prevalence. A major contributor is the consumption of high-fat diets, an increasingly common feature of modern diets. Maternal obesity results in an increased risk of offspring developing obesity and related health problems; however, the impact of maternal diet on the adipose tissue composition of offspring has not been evaluated. Here, we designed a generational diet-induced obesity study in female C57BL/6 mice that included maternal cohorts and their female offspring fed either a control diet (10% fat) or a high-fat diet (45% fat) and examined the visceral adipose proteome. Solubilizing proteins from adipose tissue is challenging due to the need for high concentrations of detergents; however, the use of a detergent-compatible sample preparation strategy based on suspension trapping (S-Trap) enabled label-free quantitative bottom-up analysis of the adipose proteome. We identified differentially expressed proteins related to lipid metabolism, inflammatory disease, immune response, and cancer, providing valuable molecular-level insight into how maternal obesity impacts the health of offspring. Data are available via ProteomeXchange with the identifier PXD042092.

**Keywords:** diet; adipose tissue; omental tissue; obesity; generational obesity; proteomics; S-Trap; suspension trapping



**Citation:** Schuster-Little, N.; McCabe, M.; Nenninger, K.; Safavi-Sohi, R.; Whelan, R.J.; Hilliard, T.S. Generational Diet-Induced Obesity Remodels the Omental Adipose Proteome in Female Mice. *Nutrients* **2024**, *16*, 3086. <https://doi.org/10.3390/nu16183086>

Academic Editor: Laura J. den Hartigh

Received: 24 July 2024

Revised: 16 August 2024

Accepted: 27 August 2024

Published: 13 September 2024



**Copyright:** © 2024 by the authors. Licensee MDPI, Basel, Switzerland. This article is an open access article distributed under the terms and conditions of the Creative Commons Attribution (CC BY) license (<https://creativecommons.org/licenses/by/4.0/>).

## 1. Introduction

In 2022, over 890 million adults were considered obese, according to the World Health Organization (WHO) [1]. Despite being a preventable disease, obesity has tripled since 1975 and is now one of the leading causes of death worldwide [1]. The increased prevalence of obesity has led to a significant rise in several diseases, including type 2 diabetes [2], cardiovascular disease [3], sleep apnea [4], and cancer [5]. Most recently, obesity has been associated with increased severity of COVID-19 illness [6,7].

A major contributor to the obesity epidemic is the Western diet, which contains energy-dense foods that are high in fat and sugar [1,7]. In laboratory studies of animal models, animal feed can be controlled to assess the effects of high-fat (Western) and low-fat (control) diets on profiles of protein expression by performing quantitative proteomics analysis on suitable tissue such as adipose [8]. Adipose tissue growth varies according to maternal diet and can contribute to metabolic disorders, such as insulin resistance and impaired glucose homeostasis [9]. While the effect of diet, both low and high fat, on protein expression in

adipose tissue has been reported [10–14], the influence of generational or maternal obesity on the remodeling of the visceral omental adipose proteome has not been evaluated.

While adipose tissue is a valuable resource for understanding the molecular-level changes resulting from dietary interventions, it is a challenging matrix for proteomics analysis because of its abundance in lipids. High concentrations of detergent are required to extract and solubilize proteins from adipose [15–17]; however, these agents are not compatible with mass spectrometry. To overcome this problem, gel-based approaches are commonly used [16,18]. Alternatively, suspension trapping (S-Traps) is a filter-based method used for proteomics sample preparation that requires high concentrations of SDS [19]. Considering the challenges of working with adipose tissue and the need for strong detergents to solubilize proteins, we hypothesized that S-Traps would be a suitable sample preparation method for adipose tissue. Here, for the first time, we utilize S-Traps to perform proteomic analysis of omental visceral adipose tissue in a female generational obesity cohort study. We have identified unique sets of proteins and protein networks that characterize changes in omental adipose in response to modulation of dam and offspring diet. Overall, the identified differentially expressed proteins were involved in pathways related to cancer, inflammatory disease, and immune response. The greatest difference in proteomic profiles was observed when comparing lean and generational obese offspring, with observed alterations in proteins associated with lipid transport, lipid metabolism, and immune response. These findings illuminate the complex biological mechanisms that regulate adipose tissue and represent a broad-based reference dataset to inform future studies of generational obesity and its impact on peritoneal diseases, including peritonitis, dialysis-associated injuries, and peritoneal metastasis of cancers, such as ovarian, gastric, and pancreatic cancer.

## 2. Materials and Methods

### 2.1. Materials

Sodium dodecyl sulfate (SDS), iodoacetamide (IAA), and triethylammonium bicarbonate (TEAB) were obtained through Millipore Sigma (St. Louis, MO, USA). Tris(2-carboxyethyl)phosphine (TCEP), deoxycholic acid (DCA), phosphoric acid, methanol (Burdick & Jackson, Muskegon, MI, USA), 0.1% formic acid in water (Burdick & Jackson, Muskegon, MI, USA), and phosphate-buffered saline (PBS) were purchased from VWR. Additionally, 99% pure formic acid (FA), acetonitrile (ACN), and C18 ZipTips were purchased from Fisher Scientific (Hanover Park, IL, USA). S-Traps™ were purchased from Protifi (Huntington, NY, USA). Mass spectrometry-grade trypsin gold was ordered from Promega (Madison, WI, USA) and reconstituted according to the manufacturer's instructions.

### 2.2. Experimental Design and Statistical Rationale

All murine studies were approved by the Institutional Animal Care and Use Committee, University of Notre Dame, and were conducted in accordance with relevant guidelines and regulations of this committee. All experiments were conducted with three biological samples per dietary cohort. Each sample was analyzed in technical duplicate for a total of six LC-MS/MS analyses per dietary cohort. Statistical analysis was carried out using Graph Pad Prism 9.0 software.

### 2.3. Murine Generational Obesity Animal Model

The pre-clinical murine model of diet-induced obesity (DIO) includes two maternal cohorts (dams) of female C57BL/6 mice (Jackson Lab) with intact host immunity fed a control diet (10% fat; control dam (Dam<sub>(CON)</sub>); Research Diets D12450H) compared to animals fed a high-fat Western diet (45% fat, western dam Dam<sub>(WES)</sub>; Research Diets D12451), as illustrated in Figure 1. All male mice (sires) were fed normal breeder's chow and allowed to mate with a pair of female mice (dams) from each diet cohort. Offspring resulting from both cohorts of dams were allocated to either the control or Western diet (Figure 1). Cohorts are designated based on Maternal Diet<sub>(OFFSPRING DIET)</sub> as follows: Lean

= Con<sub>(CON)</sub>; Transitional Lean = Con<sub>(WES)</sub>; Transitional Obesity = Wes<sub>(CON)</sub>; Generational Obese = Wes<sub>(WES)</sub>. Mice were euthanized, and the omenta were dissected [20].

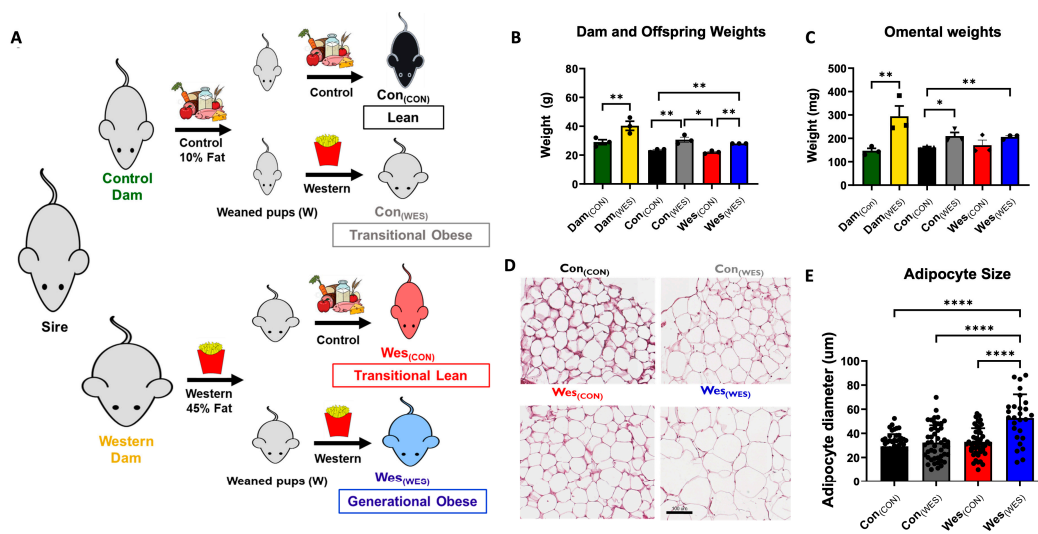


**Figure 1.** Experimental design used to investigate generational obesity and visceral adipose characteristics. (A) Control and Western diet-fed dams were bred with the same sire, and each had a litter of pups. Female offspring from the control-diet dams (Dam<sub>(CON)</sub>) were fed a control diet (10% fat) or a Western diet (45% fat), resulting in two dietary cohorts: Con<sub>(CON)</sub> and Con<sub>(WES)</sub>, respectively. Offspring from Western-diet dams (Dam<sub>(WES)</sub>) were fed either a control diet (10% fat) or a Western diet (45% fat), resulting in two dietary cohorts: Wes<sub>(CON)</sub> and Wes<sub>(WES)</sub>, respectively. All mice were sacrificed, and the omentum was excised from each animal. (B) Dam and offspring body weight at the time of omenta excision ( $n = 3$ ). (C) Omental weights from dietary cohorts at the time of excision. (D) Representative H&E staining of visceral adipose from each dietary cohort. (E) Adipocyte diameter quantified by Image J. Statistical results are presented as the mean  $\pm$  SEM.  $n = 3$  for each dietary cohort. \*  $p < 0.05$ ; \*\*  $p < 0.01$ ; \*\*\*\*  $p < 0.0001$ .

#### 2.4. Protein Isolation and Proteomics Sample Processing

Proteins were isolated from adipose tissue using the Qiagen AllPrep DNA/RNA/Protein Mini Kit (Cat No. 80004, Qiagen, Germantown, MD, USA). Isolated proteins were eluted into nuclease-free water and stored at  $-80\text{ }^{\circ}\text{C}$  until future use. Before proteolytic digestion, proteins were solubilized by adding SDS and PBS for final concentrations of 5% and 1 $\times$ , respectively. Total protein was quantified using the Pierce BCA assay.

For each digestion, 20  $\mu\text{g}$  of protein was taken into the reaction. Proteins were denatured and reduced using 7% SDS and 10 mM TCEP at  $95\text{ }^{\circ}\text{C}$  for 10 min; 0.2% DCA was included to prevent protein adsorption, and 100 mM TEAB was included as a buffering agent. Following reduction, 5 mM IAA was added, and samples were incubated in the dark for 30 min at RT. The alkylation reaction was quenched using phosphoric acid at a final concentration of 1.2%. The proteins were then prepared for S-Trap digestion following the kit's instructions. Briefly, 100 mM TEAB in MeOH was added to flocculate proteins. The suspension was spun onto the S-Trap at 4000 g for 30 s. The S-Trap was washed using 100 mM TEAB in water. Then, 1  $\mu\text{g}$  of trypsin in 100 mM TEAB in water was added to the S-Trap. The S-Trap was placed in an incubator set to  $37\text{ }^{\circ}\text{C}$  for 4 h. Following digestion, peptides were eluted using 100 mM TEAB, 0.1% FA, 50% ACN, and 0.1% FA. All eluates were collected into the same tube and quenched with formic acid to a final concentration of 1%. All eluates were collected into one vial and dried on a SpeedVac. Peptides were resuspended in 0.1% FA, desalted using ZipTips, evaporated to dryness, and resuspended in water containing 4% ACN and 0.5% FA to 20  $\mu\text{L}$ . Each sample was desalted twice for a total of 10  $\mu\text{g}$  peptide. Each sample was analyzed in technical duplicate.

### 2.5. Liquid Chromatography and Mass Spectrometry Conditions

Peptides were analyzed using a Waters M-Class ultrahigh-pressure liquid chromatography (LC) system coupled to a Q-Exactive High-Frequency (QEHF) mass spectrometer (Thermo Scientific, Waltham, MA, USA). Peptides were eluted from a BEH C18 column (Waters, 100  $\mu\text{m}$  inner diameter  $\times$  100 mm outer diameter, 1.7  $\mu\text{m}$  particle size) using a 100 min gradient at a flow rate of 0.9  $\mu\text{L}/\text{min}$ . A binary solvent system was used, where Solvent A consisted of water with 0.1% FA, while solvent B consisted of CAN with 0.1% FA (Burdick & Jackson, Muskegon, MI, USA, VWR). The following linear gradient was used for all samples: 4–33% B for 90 min, 33–80% B for 2 min, constant at 80% B for 6 min, and then 80–0% B for 2 min to equilibrate the column. Data were collected in positive ionization mode. Mass spectra were acquired in the Orbitrap at 60,000 resolving power, and tandem mass spectra were then generated for the top seventeen most abundant ions with charge states ranging between 2 and 5. Fragmentation of selected peptide ions was achieved via high-energy collisional dissociation (HCD) at a normalized collision energy of 35 eV in the HCD cell of the QEHF. Samples from three different mice were digested to generate biological triplicates. Each of these digests was analyzed in technical duplicate for a total of six LC-MS/MS analyses per dietary cohort.

### 2.6. Data Analysis

The data analysis was performed using MetaMorpheus version 0.0.320, available at <https://github.com/smith-chem-wisc/MetaMorpheus> (accessed on 29 September 2022) [21,22]. The mass spectrometry proteomics data have been deposited to the ProteomeXchange Consortium via the PRIDE [23] partner repository with the dataset identifier PXD042092. The following calibrate and search task settings were used: protease = trypsin; maximum missed cleavages = 2; minimum peptide length = 7; maximum peptide length = 45; initiator methionine behavior = Variable; fixed modifications = Carbamidomethyl on C, Carbamidomethyl on U; variable modifications = Oxidation on M, Deamidation on N, Deamidation on Q; max mods per peptide = 2; max modification isoforms = 1024; precursor mass tolerance =  $\pm 10.0000$  PPM; product mass tolerance =  $\pm 0.0200$  Absolute; report PSM ambiguity = True. The combined search database contained 55,557 non-decoy protein entries, including 474 contaminant sequences. Label-free quantification (LFQ) was performed using FlashLFQ [24]. A 20 ppm peak tolerance was allowed, and match between runs was enabled. Data files were processed on a computer running Microsoft Windows 10.0.19044 with a 64-bit AMD Ryzen Threadripper PRO 3955WX 16-Cores processor with 32 threads and 128 GB installed RAM. The total time to perform the calibrate and search tasks on 36 spectra files was 395.92 and 218.21 min, respectively.

The LFQ intensity values were used to determine changes in protein abundance, and volcano plots were generated using R-studio (version 2022.2.3.492) [25]. The average and standard deviation of the LFQ intensity values for each of the six injections per cohort were calculated. The log<sub>2</sub> fold change was calculated for each comparison group, and *p*-values were calculated using Student's *t*-test. The significance values were set as fold change >2 or <−2 and a *p*-value less than 0.05. The following R-studio packages were used for data analysis: ggplot2 [26], plotly [27], stringr [28], ggrepel [29], and tidyverse [30]. Venn diagrams were created using Venny 2.1 [31].

Principal component analysis (PCA) was used as an unsupervised method to represent a high-dimensional data structure in a smaller number of dimensions for characterizing objects in the dataset. PCA was applied to quantitative proteomic data using PLS-toolbox version 9.1 [32]. The datasets of all quantified proteins were used to perform a PCA analysis. The data points for each of the groups (i) Con<sub>(CON)</sub>; Con<sub>(WES)</sub>, (ii) Wes<sub>(CON)</sub>; Wes<sub>(WES)</sub>, and (iii) Dam<sub>(CON)</sub>; Dam<sub>(WES)</sub> were separated into two sets (offspring and dam), and PCA analysis was performed. The first three eigenvalues explained more than 85% of the total variance. The PCA score-plot obtained using the PLS-toolbox, projecting the objects into the subspace, was created by the 1st, 2nd, and 3rd latent variables of the model.

Gene ontology analysis was performed using the PANTHER (Protein ANalysis THrough Evolutionary Relationships) Classification System [33]. UniProt protein accession numbers were used as the input for analysis. Our analyses looked at biological process, cellular component, and molecular function of the genes identified in each comparison group. Pie charts were created in Igor Pro 9.0 (Wavemetrics) using the data from PANTHER.

Differentially expressed proteins ( $p < 0.05$ ) between the dietary groups were subjected to Ingenuity Pathway Analysis (IPA; Qiagen) to determine differential regulation of canonical pathways and functional enrichment analyses.

### 3. Results

#### 3.1. Generational Obesity Breeding Scheme and Characterization

A breeding scheme was designed to examine the heritable contribution of maternal high-fat diet as well as the impact of offspring diet on the omental adipose proteome (Figure 1A). Female mice (dams) were exposed to a high-fat diet (Western; Wes) or a low-fat diet (control; Con) for 6 weeks before pregnancy and until weaning of offspring at 4 weeks. A dam from each diet cohort (Dam<sub>(CON)</sub> and Dam<sub>(WES)</sub>) was bred with a male mouse (sire) and the resulting female offspring from each dam were fed either control or Western diet, resulting in four additional offspring dietary cohorts: Con<sub>(CON)</sub> (Lean); Con<sub>(WES)</sub> (transitional obese); Wes<sub>(CON)</sub> (transitional lean); and Wes<sub>(WES)</sub> (generational obese) (Figure 1A). As expected, dams fed a high-fat diet had elevated body weight compared to low-fat diet-fed dams (Figure 1B). The first-generation offspring of these dams fed a high-fat diet had an elevated body weight regardless of dam diet (Con<sub>(WES)</sub> and Wes<sub>(WES)</sub>; Figure 1B). Additionally, the omental weights of high-fat diet-fed offspring (Con<sub>(WES)</sub> and Wes<sub>(WES)</sub>) were increased when compared to mice only exposed to a control diet (Con<sub>(CON)</sub>; Figure 1C). Adipocyte hypertrophy was observed in generational obese mice (Wes<sub>(WES)</sub>) relative to all the other dietary cohorts (Figure 1D,E). To evaluate the generational dietary influence on omental adipose proteome remodeling, several comparisons were made, as shown in Table 1, with three additional comparisons shown in Table S1. Although all cohorts and groups are of interest, the primary focus of this report is on the generational obesity and maternal obesity comparison groups.

**Table 1.** Description of cohort comparisons and their given group name. Colors indicate the different dietary cohorts.

Group Name	Cohorts Compared
Generational Obesity	Con <sub>(CON)</sub> vs. Wes <sub>(WES)</sub>
Obese Maternal Influence	Wes <sub>(CON)</sub> vs. Wes <sub>(WES)</sub>
Maternal Influence	Con <sub>(CON)</sub> vs. Wes <sub>(CON)</sub>
Maternal Obesity	Dam <sub>(CON)</sub> vs. Dam <sub>(WES)</sub>

#### 3.2. Proteolytic Digestion of Omental Adipose Tissue Proteins Using S-Traps

Here, we report the first use of S-Traps to digest proteins isolated from omental adipose tissue. The data points for each of the groups (i) Con<sub>(CON)</sub>; Con<sub>(WES)</sub>, (ii) Wes<sub>(CON)</sub>; Wes<sub>(WES)</sub>, and (iii) Dam<sub>(CON)</sub>; Dam<sub>(WES)</sub> were separated into two sets (offspring and dam), and PCA analysis was performed. Both dam and offspring dietary cohorts were segregated into dietary cohorts by PCA analysis (Figure 2A–D). Using the S-Trap digestion method, we identified over 1000 proteins from most cohorts (Table 2 and Table S2; Figure 3A,B). In comparison to more traditional methods, including 2D gel electrophoresis and in-solution digestions that identify 88 and 329 proteins from mouse adipose tissue, we identified significantly more proteins [34,35]. Additionally, while the number of reported proteins here is fewer than other literature values, this study analyzes a single tissue type, whereas other groups analyze multiple tissue types and combine the results [8,36]. The data reported in Table 2 confirmed the efficacy of S-Traps for use in the sample preparation of adipose

tissue for proteomic analysis. Of interest were proteins unique to each cohort (Figure 3A,B) and proteins differentially expressed among the comparison groups (Figure 3C–H). For example, the generational obese ( $Wes_{(WES)}$ ) cohort contained 86 unique proteins (Figure 3B), of which 20 were membrane-bound proteins.

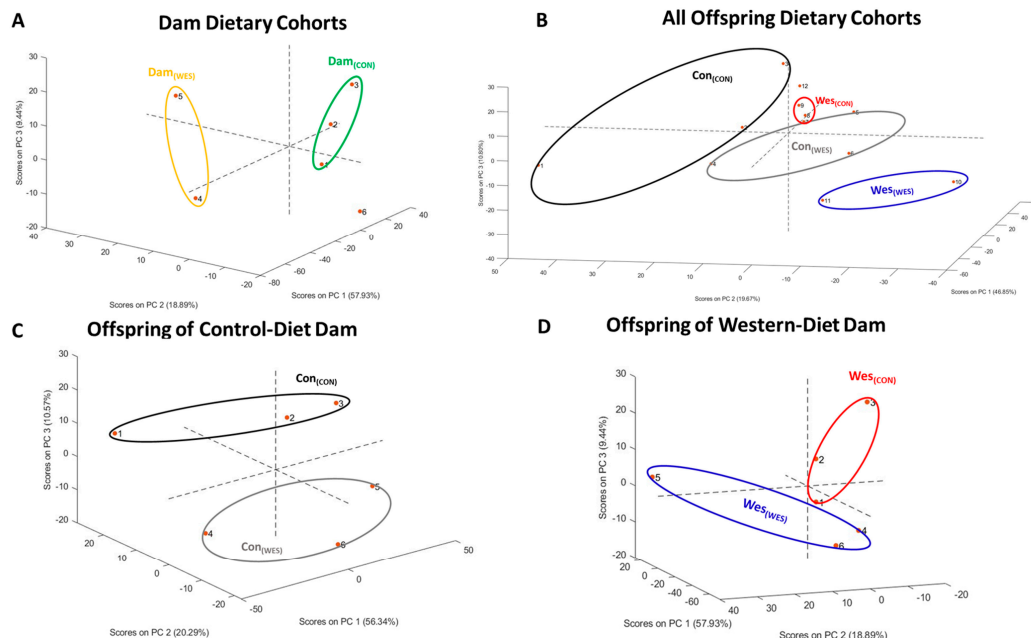


**Figure 2.** Principal component analysis (PCA) revealed clustering of various dietary cohorts. (A) Clustering of dam dietary cohorts. Dots 1–3 represents  $Dam_{(CON)}$  and 4–6 represents  $Dam_{(WES)}$ . (B) Clustering of all offspring dietary cohorts. Dots 1–3 represents  $Con_{(CON)}$ ; 4–6 represents  $Con_{(WES)}$ ; 7–9 represents  $Wes_{(CON)}$ ; and 10–12 represents  $Wes_{(WES)}$ . (C) Clustering of offspring from control-diet dam. Dots 1–3 represents  $Con_{(CON)}$  and 4–6 represents  $Con_{(WES)}$ . (D) Clustering of offspring from Western-diet dam. Dots 1–3 represents  $Wes_{(CON)}$  and 4–6 represents  $Wes_{(WES)}$ .

**Table 2.** Total number of proteins, peptides, and PSMs identified for each cohort. Values reported are average  $\pm$  one standard deviation ( $n = 6$  injections). Colors indicate the different dietary cohorts.

Cohort	Protein Group IDs	Peptide IDs	MS/MS	PSMs	Percentage of PSMs over MS/MS
$Dam_{(CON)}$	990 $\pm$ 31	7230 $\pm$ 244	34,158 $\pm$ 571	14,471 $\pm$ 758	42 $\pm$ 2
$Dam_{(WES)}$	1038 $\pm$ 110	7424 $\pm$ 895	35,133 $\pm$ 686	14,848 $\pm$ 1666	42 $\pm$ 4
$Con_{(CON)}$	1030 $\pm$ 45	8468 $\pm$ 556	35,648 $\pm$ 659	16,733 $\pm$ 1246	47 $\pm$ 3
$Con_{(WES)}$	1013 $\pm$ 69	7342 $\pm$ 812	34,798 $\pm$ 1134	14,675 $\pm$ 1509	42 $\pm$ 3
$Wes_{(CON)}$	1139 $\pm$ 24	8409 $\pm$ 252	35,428 $\pm$ 472	16,455 $\pm$ 631	46 $\pm$ 1
$Wes_{(WES)}$	1045 $\pm$ 128	7599 $\pm$ 1153	33,994 $\pm$ 3072	16,359 $\pm$ 3036	48 $\pm$ 10

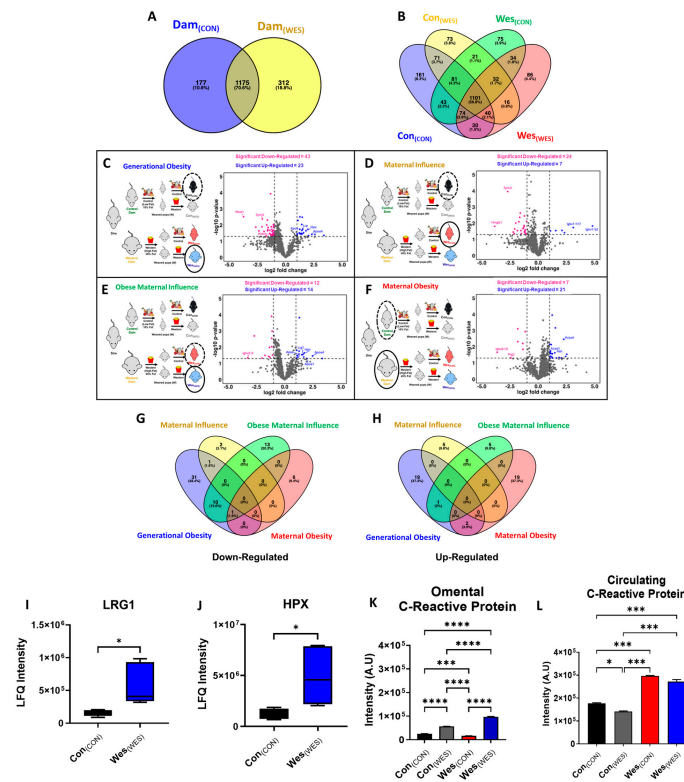


**Figure 3.** Up- and down-regulation of proteins among dietary cohorts was enabled by proteomic analysis of omental adipose. (A,B) Venn diagrams comparing omental adipose proteome for (A) dam dietary cohorts and (B) offspring cohorts. Volcano plots showing up- and down-regulated proteins for (C) generational obesity, (D) maternal influence, (E) obese maternal influence, and (F) maternal obesity. Blue dots represent up-regulated proteins, and pink dots represent down-regulated proteins. The study design to the left of each volcano plot shows the two cohorts being compared, with the solid black oval representing the fold change with respect to the cohort circled in black dotted lines. Additional volcano plots of the other groups can be found in Supplementary Figure S1. Venn diagrams of (G) down-regulated and (H) up-regulated proteins from comparison groups. Expression of two differentially expressed proteins of interest (I) LRG1 and (J) HPX between lean and generational obese dietary cohorts. Protein expression of C-reactive protein in (K) omental adipose and (L) serum from all offspring dietary cohorts. \*  $p < 0.05$ ; \*\*\*  $p < 0.001$ ; \*\*\*\*  $p < 0.0001$ .

### 3.3. Protein Expression Changes in Murine Omenta Are Diet-Dependent

To evaluate the potential for diet-induced remodeling of the omental adipose proteome, volcano plots were used to examine the differentially regulated proteins for the four comparison groups from Table 1 ( $p < 0.05$ , fold change  $\geq 1.2$ ) (Figure 3C–F). Differentially regulated proteins for the three comparison groups from Table S1 ( $p < 0.05$ , fold change  $\geq 1.2$ ) are shown in the volcano plots in Figure S1A–C. The generational obesity comparison group contained the greatest number of differentially regulated proteins out of all seven group comparisons, with 23 up-regulated and 43 down-regulated proteins in the generational obese cohort (Wes<sub>(WES)</sub>) compared to the control-only fed mice (Con<sub>(CON)</sub>) (Figure 3C). Several notable up-regulated proteins included leucine-rich alpha-2-glycoprotein 1 (LRG1; Figure 3C,I), apolipoprotein A4 (APOA4; Figures 3C and 5C), and hemopexin (HPX; Figure 3C,J). When comparing the control diet-fed cohorts (maternal influence), there were 7 up-regulated proteins and 24 down-regulated proteins (Figure 3D; Table S3), whereas offspring from obese dams (obese maternal influence) had 14 up-regulated proteins and 12 down-regulated proteins (Figure 3E; Table S3). When comparing obese dams to control dams, 21 proteins were up-regulated, and 7 proteins were down-regulated (Figure 3F; Table S3). The percentage/number of shared down-regulated or up-regulated proteins ( $p < 0.05$ ) among the different groups is shown in Figure 3G,H.

The generational obesity comparison group had 31 unique down-regulated proteins and 19 up-regulated proteins, whereas the maternal obesity comparison group had 6 unique down-regulated proteins and 19 up-regulated proteins (Figure 3G,H). Cytokine array analysis of omental adipose determined dietary differences in C-reactive protein (CRP) expression. Unexpectedly,  $Wes_{(CON)}$  mice had the lowest CRP expression, followed by  $Con_{(CON)}$  mice. Western diet-fed offspring had high CRP expression among the dietary cohorts; however, generational obese mice had the highest CRP expression in omental adipose (Figure 3K). It is noteworthy that the circulating serum CRP expression (Figure 3L) was significantly higher in offspring from Western-diet dams ( $Wes_{(CON)}$  and  $Wes_{(WES)}$ ) compared to offspring from control-diet dams ( $Con_{(CON)}$  and  $Con_{(WES)}$ ).

### 3.4. Bioinformatic Analysis of Differentially Expressed Proteins Reveals Omental Adipose Functional Differences

To investigate what biological processes, cellular components, and molecular functions were enriched by the diet-induced proteome remodeling, all significantly up- and down-regulated proteins were submitted to the PANTHER Classification System (Figures 4 and S2; Table S4). PANTHER gene ontology (GO) analysis of biological processes demonstrated that most of the generational obesity up-regulated proteins were in cellular processes (25%) and metabolic processes (26%) and represented a higher percentage of up-regulated proteins in these processes when compared to the other dietary groups (Figure 4A). Additionally, the immune system process (8%) and response to stimulus (10%) had fewer up-regulated proteins in the generational obesity group compared to the other groups. There was a similar percentage (12%) of regulated proteins enriched in biological processes involved in interspecies interaction between organisms and similar percentages (8–11%) of enriched proteins related to localization among the groups.

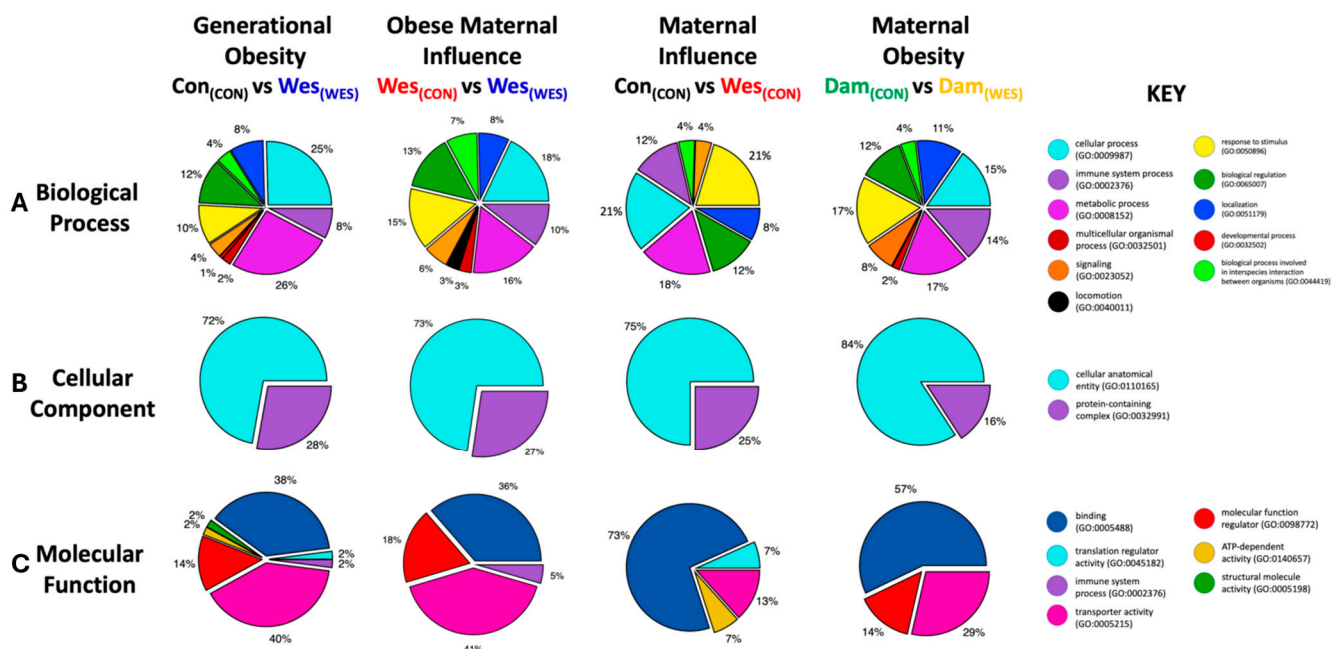


**Figure 4.** PANTHER gene ontology (GO) analysis identified the processes, location, and function associated with differentially expressed proteins. For each cohort, GO analysis identified the (A) biological process, (B) cellular component, and (C) molecular function of proteins identified by proteomics experiments.

The cellular component GO enrichment analysis only showed two significantly enriched components: cellular anatomical entity (subcellular localization) and protein-containing complex (Figure 4B). The cellular anatomical entity displayed the most up-regulated proteins across all dietary groups, with slight differences among the groups. Notably, most pro-



teins identified in all groups were localized to the extracellular space (GO:0005615) or the plasma membrane (GO:0005886; Table S4). The maternal obesity group had the fewest up-regulated proteins (16%) in the protein-containing complex (GO:0032991) compared to all other groups, which had approximately the same percentage of up-regulated proteins (25–28%).

In terms of molecular function enrichment analysis, most of the up-regulated proteins are related to binding, transporter activity, and molecular function regulation (Figure 4C). Interestingly, the generational obesity group contained functionally enriched proteins related to the aforementioned functions as well as ATP-dependent activity, structural molecule activity, translation regulator activity, and immune system response.

### 3.5. Pathway Enrichment Analysis

Canonical pathways regulated by dietary-influenced omental adipose proteins were determined by Ingenuity Pathway Analysis (IPA, Qiagen). The top 10 canonical pathways overrepresented by the differentially regulated proteins between the dietary groups are shown in Figures 5 and S3 and Table S5. Pathways associated with cancer, immune response, metabolic disease, inflammatory disease, hereditary and development disorders, and lipid and nucleic metabolism were differentially regulated in the dietary groups. In general, pathways associated with IL-15 signaling, B-cell receptor signaling, and systemic lupus erythematosus in B-cell signaling were differentially regulated in all the groups. These pathways all had an abundance of up-regulated immunoglobulin proteins.

There were twenty-six canonical pathways unique to the generational obesity group. Among the top ten canonical pathways shown in Figure 5A, the tRNA charging and maturity-onset diabetes of young (MODY) signaling, which both play a role in hereditary disorders, were exclusively overrepresented in the generational obese omenta. Four proteins—methionyl-tRNA synthetase 1 (MARS1), seryl-tRNA synthetase 1 (SARS1), threonyl-tRNA synthetase 1 (TARS1), and valyl-tRNA synthetase 1 (VARS1)—were mapped to the tRNA charging pathway (Figure 5B), and three proteins—aldolase, fructose-biphosphate B (ALDOB); apolipoprotein A4 (APOA4); and apolipoprotein E (APOE)—were mapped to the MODY signaling pathway (Figure 5C). Additionally, the IL-7 signaling pathway, which plays a role in cellular immune response, was exclusively overrepresented in the generational obesity group. Three immunoglobulin proteins were mapped to the IL-7 pathway (Table S5). The maternal influence group had twenty-three canonical pathways that were unique to this group. Heat shock protein 90 alpha family class A member 1 (HSP90AA1) and heat shock protein 90 alpha family class B member 1 (HSP90AB1) were mapped to twenty-two of the twenty-three overrepresented pathways. From the top ten canonical pathways overrepresented, five pathways were exclusively overrepresented in the maternal influence group and play a role in cancer, immunological disease, cell cycle, and vitamin and mineral metabolism (Figure 5D). The maternal obesity comparison group had twelve canonical pathways overrepresented, of which four were unique to only this group (Figure 5E). These exclusively overrepresented canonical pathways are involved in metabolic pathways, the immune response, endocrine system development, developmental/hereditary disorders, and fatty acid  $\beta$ -oxidation I pathway, which has been considered a cause in the development of obesity and metabolic diseases, including diabetes mellitus [37]. The proteins mapped to the four unique pathways were phenylalanine-4-hydroxylase (PAH), Pterin-4-alpha-carbinolamine dehydratase (PCBD1; Figure 5F), bone marrow proteoglycan (PRG2; Figure 5G), and 3-ketoacyl-CoA thiolase A (ACAA1; Figure 5H). The obese maternal influence group had five unique canonical pathways that are involved in diabetes mellitus, cancer, and metastasis (Figure 5I).

The generational obesity, obese maternal influence, and maternal obesity groups all have overrepresented FXR/RXR and LXR/RXR canonical pathways. These pathways play a role in inflammatory and lipid metabolism. The generational obesity and obese maternal influence groups had three canonical pathways overrepresented in common

that are involved in cancer, inflammatory disease, vitamin and mineral metabolism, and tissue development.

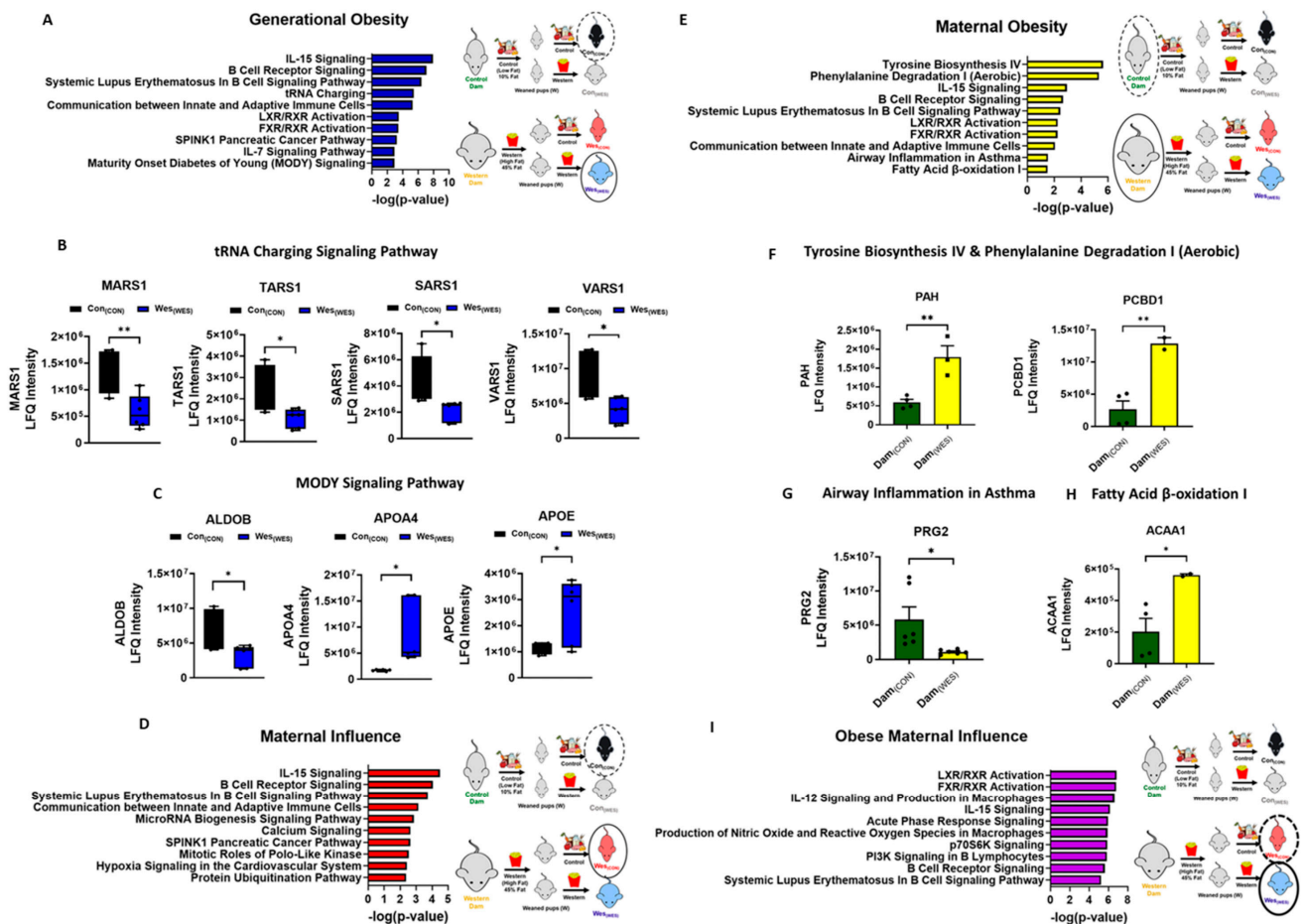


**Figure 5.** Analysis of differentially expressed proteins. (A) Ingenuity pathway analysis of differentially regulated proteins among the generational obesity comparison group. (B) Differentially expressed proteins mapped to the tRNA charging signaling pathway. (C) Differentially expressed proteins mapped to the MODY signaling pathway. Ingenuity pathway analysis of differentially regulated proteins among the (D) maternal influence and (E) maternal obesity groups. Differentially expressed proteins mapped to the (F) tyrosine biosynthesis and phenylalanine degradation signaling pathway. (G) Airway inflammation in asthma signaling pathway and (H) fatty acid  $\beta$ -oxidation I signaling pathway. (I) Ingenuity pathway analysis of differentially regulated proteins among the obese maternal influence groups. The top 10 pathways are represented in the ingenuity pathway analysis figures. \*  $p < 0.05$ ; \*\*  $p < 0.01$ .

### 4. Discussion

This study offers a global and unbiased proteomic analysis of visceral omental adipose from dietary cohorts to define molecular features of proteome remodeling that may promote functional changes in female mice. The omentum is a specialized adipose tissue that controls peritoneal homeostasis and is the preferred site of metastasis in several cancers, including gastric, pancreatic, and ovarian cancer [38–42]. Several pre-clinical studies have addressed diet influences on white adipose depots by proteomic analysis [43–46]; however, these studies pooled various distinct depots together or used male murine samples. Unlike previous studies that have investigated male offspring of obese dams, this study investigates female offspring from both obese and lean dams fed either a control low-fat diet or a Western high-fat diet, resulting in four relevant and distinct cohorts for comparison.

Sex differences have been observed between male and female adipose and are potentially due to the X and Y chromosome influences and sex hormone differences, suggesting the importance of investigating both female and male adipose [47,48]. This study is the first to assess female offspring omental adipose from four dietary cohorts to understand the combined impact of maternal and offspring diet on adipose structure and function. Our results support several lines of evidence indicating that a high-fat diet increases visceral adipose mass and adipocyte size [49–51]. Adipocyte size is mainly dependent on the triglyceride content [52]. The adipocyte hypertrophy observed in the generational obese cohort supports an increase in triglyceride content and concern regarding the long-term health implications of the generational consumption of high-fat diets. Studies have established a close association between insulin resistance and dyslipidemia with an increase in adipocyte cell size in humans, which highlights the need for effective dietary interventions to mitigate these conditions [49]. Interestingly, while the omental weights of offspring fed a Western diet were similar, there was no corresponding increase in adipocyte size in the transitional obese offspring. This disparity may be attributed to a protective effect resulting from the dam's diet. Overall, this study provides new insights into the complex relationship between diet and adipose tissue development in female offspring, with important implications for public health.

The use of S-Traps during sample preparation enabled efficient digestion of proteins, including membrane proteins, from the omenta. Using lysate from colorectal cancer cells as the input material, Hummon and co-workers compared the S-Trap sample preparation method to in-solution and FASP workflows and found that the S-Trap method identified the most proteins and peptides [53]. Elinger et al. found that S-Traps are compatible with typical protein extraction buffers and detergents [54]. Typically, membrane proteins are difficult to extract and digest due to their hydrophobic properties, which necessitates high detergent concentrations to mimic the lipid-rich environment of the membrane. Using S-Traps, we identified over 1000 proteins in every dietary cohort and a total of 115 differentially expressed proteins between the groups, of which 64 were down-regulated, and 51 were up-regulated. The use of S-Traps allowed for the identification of 15–73 membrane-bound proteins in each dietary cohort, suggesting S-Traps are superior in adipose protein extraction compared to FASP, which did not detect membrane-bound proteins [51]. PCA analysis indicated the dietary cohorts were readily distinguished. Our study demonstrated the generational obesity comparison group (lean vs. generational obese) had the greatest number of differentially regulated proteins out of all seven group comparisons, suggesting an additive effect passed through generations from an obese mother to her obese offspring. The proteins identified from omental adipose from generational obese offspring were more active in cellular and metabolic processes. Conversely, the number of overexpressed proteins involved in the immune system processes was lower in this group compared to all other comparisons. Importantly, studies have shown that obesity is associated with impaired immune function, with recent findings recognizing adipose tissue as an immune organ, emphasizing a vital role in the functioning of the immune system [55].

LRG1 and HPX were among the twenty-three up-regulated proteins in the generational obesity comparison group. LRG1 is a multi-functional circulating adipokine that is secreted by adipose tissue and promotes lipogenesis [56]. HPX is a glycoprotein that is involved in regulating inflammation and plays a role in adipogenesis and adipocyte differentiation [57,58]. CRP is a nonspecific marker of inflammation and is significantly increased in obese patients. CRP is positively associated with an increased risk of insulin resistance and diabetes in both adolescents and adults [56]. Cytokine array analysis of omental adipose confirmed a significantly elevated level of CRP in generational obese mice compared to the other dietary cohorts. This finding suggests that obesity across generations has a cumulative effect on CRP expression levels, leading to increased inflammation and, consequently, increased risk of developing obesity-associated disorders. Interestingly, high levels of CRP are positively correlated with an increase in LRG1 and HPX, suggesting the potential interplay between these proteins in the context of obesity [56,59]. Suppressing

the expression and function of either LRG1 or HPX presents a promising strategy for combating obesity and obesity-related metabolic diseases. This approach could lead to innovative and targeted interventions designed to address the health challenges associated with these conditions.

IL-15 signaling, B-cell receptor signaling, and systemic lupus erythematosus in B-cell signaling were differentially regulated among all the groups. These pathways had an abundance of immunoglobulin proteins that were up-regulated. The production of proinflammatory immunoglobulins has been linked to B-cell-mediated inflammation. It has been suggested that a high-fat diet induces changes in the immunoglobulin heavy chain supply in B cells of adipose tissue [60]. B cells infiltrate visceral adipose, causing functional and phenotypic changes in response to diet-induced obesity. Additionally, B cells govern systemic and local adipose tissue inflammation, as well as obesity-related insulin resistance [61,62]. These findings suggest that B cells play a pivotal role in obesity-induced inflammation and associated diseases.

An unexpected finding from this study was that tRNA charging represents one of the most pronounced differences unique to the generational obesity group. Transfer RNA (tRNA) charging is created by the linkage of an amino acid and a tRNA, resulting in an aminoacyl-tRNA for each amino acid, and it must occur to initiate translation and protein synthesis [63]. Both genetic and environmental effects on tRNAs, causing tRNA aminoacylation, modification, and fragmentation, have emerged as novel contributors to diabetes and obesity. Interestingly, diet-induced tRNA fragments have been linked to the intergenerational inheritance of metabolic traits, indicating that maternal lifestyle choices and habits can have long-lasting effects on the health of offspring [63,64].

Overrepresentation in the MODY signaling pathway was also exclusive to the generational obesity group. MODY is a rare form of familial diabetes mellitus that is usually diagnosed in young adulthood [65–67]. Among proteins in the MODY pathway, ALDOB expression was decreased in generational obese mice. ALDOB is an enzyme involved in fructose metabolism that also plays a role in gluconeogenesis and glycolysis [68]. ALDOB deficiency in humans causes an accumulation of fructose-1-phosphate that subsequently leads to hypoglycemia. Furthermore, ALDOB deficiency has been shown to cause hepatic fat accumulation in humans [69], as well as hereditary fructose intolerance, which ultimately leads to liver failure [70]. The reduction of this enzyme in the  $Wes_{(WES)}$  offspring suggests a detrimental consequence of generational obesity.

Both APOA4 and APOE were increased in the generational obese ( $Wes_{(WES)}$ ) cohort compared to the lean ( $Con_{(CON)}$ ) cohort. APOA4 is the most abundant apolipoprotein that facilitates lipid transport and metabolism. APOA4 is synthesized in the small intestine and transported by circulation to the adipose, among other tissues. APOA4 is involved in several aspects of glucose homeostasis, including the promotion of glucose uptake in adipocytes [71], and is proposed to be an early diagnostic biomarker of prediabetes [72], impaired renal function [73], and liver fibrosis [74,75]. APOE is a multi-functional protein highly expressed in adipose tissue, where it modulates adipocyte lipid influx. The overexpression of APOE has been shown to predispose mice to diet-induced obesity, hyperglycemia, and insulin resistance, suggesting generational obese mice ( $Wes_{(WES)}$ ) have a high propensity for developing hyperglycemia and insulin resistance [76,77]. Additionally, the overexpression of APOE has also been associated with tumor progression and poor survival, which could play a role in cancers that develop in the peritoneal cavity or metastasize to the adipose-rich omentum [78,79].

PAH, PCBD1, and ACAA1 were increased in high-fat diet-fed dams ( $Dam_{(WES)}$ ) compared to low-fat diet-fed dams ( $Dam_{(CON)}$ ). PCBD1 is an enzyme responsible for recycling tetrahydrobiopterin. Tetrahydrobiopterin works with PAH to convert phenylalanine to tyrosine. A deficiency in the PAH enzyme leads to hyperphenylalaninemia, a recessive inherited metabolic condition [80,81]. Increased circulating concentrations of phenylalanine and tyrosine have both been reported to be increased in the obese and in type 2 diabetes. PRG2 was down-regulated in obese dams compared to lean dams. PRG2 is the predomi-

nant component of the eosinophil leukocyte granule. Adipose eosinophils are reduced in obesity [82], and an increase in eosinophils prevented high-fat diet-induced weight gain, suggesting that therapeutic targeting of adipose eosinophils may reduce inflammation and body fat [83]. Additionally, low PRG2 expression has been associated with drug resistance in chronic myeloid leukemia [84]. ACAA1 is a key regulator of fatty acid  $\beta$ -oxidation in peroxisomes and lipid metabolism. Its function is to catalyze the cleavage of 3-ketoacyl-CoA to acetyl-CoA and acyl-CoA, which contribute to the synthesis and degradation of fatty acids [85]. ACAA1 plays a role in positively regulating cell viability, lipogenesis, and triglyceride accumulation [86].

## 5. Conclusions

Maternal obesity is a global public health concern that affects the short- and long-term health of the mother and offspring. The increase in the prevalence of childhood obesity is also a major concern, as the onset of obesity can be influenced by both environmental and genetic factors. Fetal overgrowth in human pregnancy is often the result of maternal obesity and is a risk factor for developing obesity later in life (generational obesity) [87]. Furthermore, maternal obesity may play a direct role in the transmission of obesity-related traits from generation to generation [88]. This study provides an unbiased proteomic analysis of the omental adipose proteome from distinct maternal and offspring dietary cohorts and reveals that generational obesity is a detrimental phenomenon that warrants further investigation. The data collected herein provide a valuable resource and novel insight into the role of generational obesity on the peritoneal cavity, specifically the adipose-rich omentum. Further exploration of the differentially expressed proteins is warranted, as a better understanding of the impact of generational obesity on the omentum will help improve the characterization of obesity and its associated health conditions and will aid in the discovery of therapeutic interventions that will ultimately improve outcomes and quality of life for those affected by these conditions.

**Supplementary Materials:** The following supporting information can be downloaded at: <https://www.mdpi.com/article/10.3390/nu16183086/s1>, Figure S1. Proteomic analysis of omental adipose. Figure S2. PANTHER gene ontology. Figure S3. Pathway analysis of differentially expressed proteins. Table S1. Additional comparison groups. Table S2. Proteins groups from each cohort. Table S3. Up- and down-regulated proteins. Table S4. PANTHER raw data for all comparison groups. Table S5. IPA canonical pathway analysis for all groups.

**Author Contributions:** Conceptualization, T.S.H.; Investigation, N.S.-L., M.M., K.N., R.S.-S. and T.S.H.; Methodology, Formal Analysis, Writing—original draft, Visualization, N.S.-L. and T.S.H.; Writing—review and editing, N.S.-L., R.S.-S., R.J.W. and T.S.H.; Funding Acquisition, N.S.-L., R.S.-S., R.J.W. and T.S.H.; Supervision, R.J.W. and T.S.H. All authors have read and agreed to the published version of the manuscript.

**Funding:** This work was supported in part by research grant K01 CA218305 (T.S.H.) from the National Institutes of Health, National Cancer Institute. N.S.L. was a fellow of the Chemistry-Biochemistry-Biology Interface (CBBI) Program at the University of Notre Dame, supported by training grant T32GM075762 from the National Institute of General Medical Sciences. R.S. acknowledges support from Walther Cancer Foundation, Harper Cancer Research Institute Cancer Cure Ventures Award number 0184.01. R.J.W. acknowledges support from the University of Notre Dame and the University of Kansas. The content is solely the responsibility of the authors and does not necessarily represent the official views of the National Institute of General Medical Sciences or the National Institutes of Health.

**Data Availability Statement:** The mass spectrometry proteomics datasets generated for this study can be found in the ProteomeXchange Consortium via the PRIDE partner repository with the dataset identifier PXD042092.

**Acknowledgments:** The authors wish to thank Bill Boggess and the University of Notre Dame Mass Spectrometry and Proteomics Facility (MSPF) for expert technical assistance. We also thank Simon Weaver for help in developing R scripts to create volcano plots.

**Conflicts of Interest:** The authors declare no conflicts of interest.

## References

1. WHO. Obesity and Overweight [Fact Sheet]. 2024. Available online: <https://www.who.int/news-room/fact-sheets/detail/obesity-and-overweight> (accessed on 7 September 2022).
2. Paczkowska-Abdulsalam, M.; Kretowski, A. Obesity, metabolic health and omics: Current status and future directions. *World J. Diabetes* **2021**, *12*, 420–436. [[CrossRef](#)] [[PubMed](#)]
3. Duflou, J.; Virmani, R.; Rabin, I.; Burke, A.; Farb, A.; Smialek, J. Sudden death as a result of heart disease in morbid obesity. *Am. Heart J.* **1995**, *130*, 306–313. [[CrossRef](#)] [[PubMed](#)]
4. Gnessi, L.; Mariani, S.; Fiore, D.; Varone, L.; Basciani, S.; Persichetti, A.; Watanabe, M.; Saponara, M.; Spera, G.; Moretti, C. Obstructive sleep apnea and bone mineral density in obese patients. *Diabetes Metab. Syndr. Obes.* **2012**, *5*, 395–401. [[CrossRef](#)]
5. Friedenreich, C.M.; Ryder-Burbidge, C.; McNeil, J. Physical activity, obesity and sedentary behavior in cancer etiology: Epidemiologic evidence and biologic mechanisms. *Mol. Oncol.* **2021**, *15*, 790–800. [[CrossRef](#)]
6. Busetto, L.; Bettini, S.; Fabris, R.; Serra, R.; Pra, C.D.; Maffei, P.; Rossato, M.; Fioretto, P.; Vettor, R. Obesity and COVID-19: An Italian Snapshot. *Obesity* **2020**, *28*, 1600–1605. [[CrossRef](#)]
7. Rakhra, V.; Galappaththy, S.L.; Bulchandani, S.; Cabandugama, P.K. Obesity and the Western Diet: How We Got Here. *Mo. Med.* **2020**, *117*, 536–538.
8. Feist, P.E.; Loughran, E.A.; Stack, M.S.; Hummon, A.B. Quantitative proteomic analysis of murine white adipose tissue for peritoneal cancer metastasis. *Anal. Bioanal. Chem.* **2018**, *410*, 1583–1594. [[CrossRef](#)]
9. Symonds, M.E.; Pope, M.; Sharkey, D.; Budge, H. Adipose tissue and fetal programming. *Diabetologia* **2012**, *55*, 1597–1606. [[CrossRef](#)] [[PubMed](#)]
10. Schmid, G.M.; Converset, V.; Walter, N.; Sennitt, M.V.; Leung, K.Y.; Byers, H.; Ward, M.; Hochstrasser, D.F.; Cawthorne, M.A.; Sanchez, J.C. Effect of high-fat diet on the expression of proteins in muscle, adipose tissues, and liver of C57BL/6 mice. *Proteomics* **2004**, *4*, 2270–2282. [[CrossRef](#)]
11. Jiang, L.; Wang, Q.; Yu, Y.; Zhao, F.; Huang, P.; Zeng, R.; Qi, R.Z.; Li, W.; Liu, Y. Leptin contributes to the adaptive responses of mice to high-fat diet intake through suppressing the lipogenic pathway. *PLoS ONE* **2009**, *4*, e6884. [[CrossRef](#)]
12. Xie, W.-D.; Wang, H.; Zhang, J.-F.; Kung, H.-F.; Zhao, Y.-N.; Zhang, Y. Proteomic profile of visceral adipose tissues between low-fat diet-fed obesity-resistant and obesity-prone C57BL/6 mice. *Mol. Med. Rep.* **2010**, *3*, 1047–1052. [[CrossRef](#)] [[PubMed](#)]
13. Joo, J.I.; Oh, T.S.; Kim, D.H.; Choi, D.K.; Wang, X.; Choi, J.; Yun, J.W. Differential expression of adipose tissue proteins between obesity-susceptible and -resistant rats fed a high-fat diet. *Proteomics* **2011**, *11*, 1429–1448. [[CrossRef](#)] [[PubMed](#)]
14. Mukherjee, R.; Choi, J.-W.; Choi, D.K.; Oh, T.S.; Liu, H.; Yun, J.W. Gender-dependent protein expression in white adipose tissues of lean and obese rats fed a high fat diet. *Cell. Physiol. Biochem.* **2012**, *29*, 617–634. [[CrossRef](#)] [[PubMed](#)]
15. Peral, B.; Camafeita, E.; Fernandez-Real, J.M.; Lopez, J.A. Tackling the human adipose tissue proteome to gain insight into obesity and related pathologies. *Expert Rev. Proteom.* **2009**, *6*, 353–361. [[CrossRef](#)]
16. Pasing, Y.; Colnoe, S.; Hansen, T. Proteomics of hydrophobic samples: Fast, robust and low-cost workflows for clinical approaches. *Proteomics* **2017**, *17*, 1500462. [[CrossRef](#)]
17. Khudyakov, J.I.; Deyarmin, J.S.; Hekman, R.M.; Busqueta, L.P.; Maan, R.; Mody, M.J.; Banerjee, R.; Crocker, D.E.; Champagne, C.D. A sample preparation workflow for adipose tissue shotgun proteomics and proteogenomics. *Biol. Open* **2018**, *7*, bio036731. [[CrossRef](#)]
18. Gómez-Serrano, M.; Camafeita, E.; García-Santos, E.; López, J.A.; Rubio, M.A.; Sánchez-Pernaute, A.; Torres, A.; Vázquez, J.; Peral, B. Proteome-wide alterations on adipose tissue from obese patients as age-, diabetes- and gender-specific hallmarks. *Sci. Rep.* **2016**, *6*, 25756. [[CrossRef](#)]
19. Zougman, A.; Selby, P.J.; Banks, R.E. Suspension trapping (STrap) sample preparation method for bottom-up proteomics analysis. *Proteomics* **2014**, *14*, 1000–1006. [[CrossRef](#)]
20. Harper, E.I.; Hilliard, T.S. In Vivo and Ex Vivo Analysis of Omental Adhesion in Ovarian Cancer. *Methods Mol. Biol.* **2022**, *2424*, 199–216.
21. Wenger, C.D.; Coon, J.J. A proteomics search algorithm specifically designed for high-resolution tandem mass spectra. *J. Proteome Res.* **2013**, *12*, 1377–1386. [[CrossRef](#)]
22. Solntsev, S.K.; Shortreed, M.R.; Frey, B.L.; Smith, L.M. Enhanced Global Post-translational Modification Discovery with MetaMorpheus. *J. Proteome Res.* **2018**, *17*, 1844–1851. [[CrossRef](#)] [[PubMed](#)]
23. Perez-Riverol, Y.; Bai, J.; Bandla, C.; García-Seisdedos, D.; Hewapathirana, S.; Kamatchinathan, S.; Kundu, D.J.; Prakash, A.; Frericks-Zipper, A.; Eisenacher, M.; et al. The PRIDE database resources in 2022: A hub for mass spectrometry-based proteomics evidences. *Nucleic Acids Res.* **2022**, *50*, D543–D552. [[CrossRef](#)] [[PubMed](#)]
24. Millikin, R.J.; Solntsev, S.K.; Shortreed, M.R.; Smith, L.M. Ultrafast Peptide Label-Free Quantification with FlashLFQ. *J. Proteome Res.* **2018**, *17*, 386–391. [[CrossRef](#)] [[PubMed](#)]
25. R Studio Team. *RStudio: Integrated Development for R*; Rstudio Team, PBC: Boston, MA, USA, 2020. Available online: <http://www.rstudio.com> (accessed on 16 August 2022).
26. Wickham, H.; Wickham, H. Programming with ggplot2. In *Ggplot2: Elegant Graphics for Data Analysis*; Springer: Berlin/Heidelberg, Germany, 2016; pp. 241–253.

27. Sievert, C. *Interactive Web-Based Data Visualization with R, Plotly, and Shiny*; CRC Press, Taylor and Francis Group: Boca Raton, FL, USA, 2020.
28. Wickham, H. *stringr: Simple, Consistent Wrappers for Common String Operations*. R Package Version 1.4.0. 2019. Available online: <https://github.com/tidyverse/stringr> (accessed on 16 August 2022).
29. Slowikowski, K.; Schep, A.; Hughes, S.; Dang, T.K.; Lukauskas, S.; Irisson, J.O.; Kamvar, Z.N.; Thompson, R.; Dervieux, C.; Yutabi, H.; et al. Ggrepel: Automatically Position Non-Overlapping Text Labels with 'ggplot2'. Available online: <https://ggrepel.slowkow.com/> (accessed on 30 September 2022).
30. Wickham, H.; Averick, M.; Bryan, J.; Chang, W.; McGowan, L.D.A.; François, R.; Grolemund, G.; Hayes, A.; Henry, L.; Hester, J.; et al. Welcome to the Tidyverse. *J. Open Source Softw.* **2019**, *4*, 1686. [\[CrossRef\]](#)
31. Oliveros, J.C. *An Interactive Tool for Comparing Lists with Venn Diagrams*; VENNY, 2007. Available online: <https://bioinfogp.cnb.csic.es/tools/venny/index.html> (accessed on 30 September 2022).
32. Math Works Inc. *MATLAB: The Language of Technical Computing: Computation, Visualization, Programming: Installation Guide for UNIX Version 5*; Math Works Inc.: Natick, MA, USA, 2014.
33. Thomas, P.D.; Ebert, D.; Muruganujan, A.; Mushayahama, T.; Albou, L.; Mi, H. PANTHER: Making genome-scale phylogenetics accessible to all. *Protein Sci.* **2022**, *31*, 8–22. [\[CrossRef\]](#)
34. Tomé-Carneiro, J.; Crespo, M.C.; García-Calvo, E.; Luque-García, J.L.; Dávalos, A.; Visioli, F. Proteomic evaluation of mouse adipose tissue and liver following hydroxytyrosol supplementation. *Food Chem. Toxicol.* **2017**, *107 Pt A*, 329–338. [\[CrossRef\]](#)
35. Ke, M.; Wu, H.; Zhu, Z.; Zhang, C.; Zhang, Y.; Deng, Y. Differential proteomic analysis of white adipose tissues from T2D KKAY mice by LC-ESI-QTOF. *Proteomics* **2017**, *17*, 1600219. [\[CrossRef\]](#) [\[PubMed\]](#)
36. Meierhofer, D.; Weidner, C.; Sauer, S. Integrative analysis of transcriptomics, proteomics, and metabolomics data of white adipose and liver tissue of high-fat diet and rosiglitazone-treated insulin-resistant mice identified pathway alterations and molecular hubs. *J. Proteome Res.* **2014**, *13*, 5592–5602. [\[CrossRef\]](#)
37. Shao, D.; Kolwicz, S.C., Jr.; Wang, P.; Roe, N.D.; Villet, O.; Nishi, K.; Hsu, Y.-W.A.; Flint, G.V.; Caudal, A.; Wang, W.; et al. Increasing Fatty Acid Oxidation Prevents High-Fat Diet-Induced Cardiomyopathy Through Regulating Parkin-Mediated Mitophagy. *Circulation* **2020**, *142*, 983–997. [\[CrossRef\]](#)
38. Kersy, O.; Loewenstein, S.; Lubezky, N.; Sher, O.; Simon, N.B.; Klausner, J.M.; Lahat, G. Omental Tissue-Mediated Tumorigenesis of Gastric Cancer Peritoneal Metastases. *Front. Oncol.* **2019**, *9*, 1267. [\[CrossRef\]](#)
39. Liu, Y.; Yang, J.; Hilliard, T.S.; Wang, Z.; Johnson, J.; Wang, W.; Harper, E.I.; Ott, C.; O'Brien, C.; Campbell, L.; et al. Host obesity alters the ovarian tumor immune microenvironment and impacts response to standard of care chemotherapy. *J. Exp. Clin. Cancer Res.* **2023**, *42*, 165. [\[CrossRef\]](#) [\[PubMed\]](#)
40. Feygenzon, V.; Loewenstein, S.; Lubezky, N.; Pasmanic-Chor, M.; Sher, O.; Klausner, J.M.; Lahat, G. Unique cellular interactions between pancreatic cancer cells and the omentum. *PLoS ONE* **2017**, *12*, e0179862. [\[CrossRef\]](#) [\[PubMed\]](#)
41. Motohara, T.; Masuda, K.; Morotti, M.; Zheng, Y.; El-Sahhar, S.; Chong, K.Y.; Wietek, N.; Alsaadi, A.; Carrami, E.M.; Hu, Z.; et al. An evolving story of the metastatic voyage of ovarian cancer cells: Cellular and molecular orchestration of the adipose-rich metastatic microenvironment. *Oncogene* **2019**, *38*, 2885–2898. [\[CrossRef\]](#)
42. Harper, E.I.; Hilliard, T.S.; Sheedy, E.F.; Carey, P.; Wilkinson, P.; Siroky, M.D.; Yang, J.; Agadi, E.; Leonard, A.K.; Low, E.; et al. Another wrinkle with age: Aged collagen and intra-peritoneal metastasis of ovarian cancer. *Aging Cancer* **2022**, *3*, 116–129. [\[CrossRef\]](#)
43. Harney, D.J.; Cielech, M.; Chu, R.; Cooke, K.C.; James, D.E.; Stöckli, J.; Larance, M. Proteomics analysis of adipose depots after intermittent fasting reveals visceral fat preservation mechanisms. *Cell Rep.* **2021**, *34*, 108804. [\[CrossRef\]](#)
44. Plubell, D.L.; Wilmarth, P.A.; Zhao, Y.; Fenton, A.M.; Minnier, J.; Reddy, A.P.; Klimek, J.; Yang, X.; David, L.L.; Pamir, N. Extended Multiplexing of Tandem Mass Tags (TMT) Labeling Reveals Age and High Fat Diet Specific Proteome Changes in Mouse Epididymal Adipose Tissue. *Mol. Cell. Proteom.* **2017**, *16*, 873–890. [\[CrossRef\]](#)
45. Raajendiran, A.; Krisp, C.; De Souza, D.P.; Ooi, G.; Burton, P.R.; Taylor, R.A.; Molloy, M.P.; Watt, M.J. Proteome analysis of human adipocytes identifies depot-specific heterogeneity at metabolic control points. *Am. J. Physiol. Endocrinol. Metab.* **2021**, *320*, E1068–E1084. [\[CrossRef\]](#) [\[PubMed\]](#)
46. Madsen, S.; Nelson, M.E.; Deshpande, V.; Humphrey, S.J.; Cooke, K.C.; Howell, A.; Diaz-Vegas, A.; Burchfield, J.G.; Stöckli, J.; James, D.E. Deep Proteome Profiling of White Adipose Tissue Reveals Marked Conservation and Distinct Features between Different Anatomical Depots. *Mol. Cell. Proteom.* **2023**, *22*, 100508. [\[CrossRef\]](#)
47. Arnold, A.P.; Cassis, L.A.; Eghbali, M.; Reue, K.; Sandberg, K. Sex Hormones and Sex Chromosomes Cause Sex Differences in the Development of Cardiovascular Diseases. *Arterioscler. Thromb. Vasc. Biol.* **2017**, *37*, 746–756. [\[CrossRef\]](#)
48. Chen, X.; McClusky, R.; Chen, J.; Beaven, S.W.; Tontonoz, P.; Arnold, A.P.; Reue, K. The number of x chromosomes causes sex differences in adiposity in mice. *PLoS Genet.* **2012**, *8*, e1002709. [\[CrossRef\]](#)
49. Veilleux, A.; Caron-Jobin, M.; Noel, S.; Laberge, P.Y.; Tchernof, A. Visceral adipocyte hypertrophy is associated with dyslipidemia independent of body composition and fat distribution in women. *Diabetes* **2011**, *60*, 1504–1511. [\[CrossRef\]](#) [\[PubMed\]](#)
50. Hoffstedt, J.; Arner, E.; Wahrenberg, H.; Andersson, D.P.; Qvisth, V.; Löfgren, P.; Rydén, M.; Thörne, A.; Wirén, M.; Palmér, M.; et al. Regional impact of adipose tissue morphology on the metabolic profile in morbid obesity. *Diabetologia* **2010**, *53*, 2496–2503. [\[CrossRef\]](#)

51. Zhu, R.; Chen, S. Proteomic analysis reveals semaglutide impacts lipogenic protein expression in epididymal adipose tissue of obese mice. *Front. Endocrinol.* **2023**, *14*, 1095432. [[CrossRef](#)]
52. Stenkula, K.G.; Erlanson-Albertsson, C. Adipose cell size: Importance in health and disease. *Am. J. Physiol. Regul. Integr. Comp. Physiol.* **2018**, *315*, R284–R295. [[CrossRef](#)]
53. Ludwig, K.R.; Schroll, M.M.; Hummon, A.B. Comparison of In-Solution, FASP, and S-Trap Based Digestion Methods for Bottom-Up Proteomic Studies. *J. Proteome Res.* **2018**, *17*, 2480–2490. [[CrossRef](#)]
54. Elinger, D.; Gabashvili, A.; Levin, Y. Suspension Trapping (S-Trap) Is Compatible with Typical Protein Extraction Buffers and Detergents for Bottom-Up Proteomics. *J. Proteome Res.* **2019**, *18*, 1441–1445. [[CrossRef](#)] [[PubMed](#)]
55. Schmidt, V.; Hogan, A.E.; Fallon, P.G.; Schwartz, C. Obesity-Mediated Immune Modulation: One Step Forward, (Th)2 Steps Back. *Front. Immunol.* **2022**, *13*, 932893. [[CrossRef](#)] [[PubMed](#)]
56. Alhammad, R.; Abu-Farha, M.; Hammad, M.M.; Thanaraj, T.A.; Channanath, A.; Alam-Eldin, N.; Al-Sabah, R.; Shaban, L.; Alduraywish, A.; Al-Mulla, F.; et al. Increased LRG1 Levels in Overweight and Obese Adolescents and Its Association with Obesity Markers, Including Leptin, Chemerin, and High Sensitivity C-Reactive Protein. *Int. J. Mol. Sci.* **2022**, *23*, 8564. [[CrossRef](#)]
57. Tolosano, E.; Altruda, F. Hemopexin: Structure, function, and regulation. *DNA Cell Biol.* **2002**, *21*, 297–306. [[CrossRef](#)]
58. Lawson, H.A.; Zayed, M.; Wayhart, J.P.; Fabbrini, E.; Love-Gregory, L.; Klein, S.; Semenkovich, C.F. Physiologic and genetic evidence links hemopexin to triglycerides in mice and humans. *Int. J. Obes.* **2017**, *41*, 631–638. [[CrossRef](#)]
59. Winter, N.A.; Gibson, P.G.; Fricker, M.; Simpson, J.L.; Wark, P.A.; McDonald, V.M. Hemopexin: A Novel Anti-inflammatory Marker for Distinguishing COPD From Asthma. *Allergy Asthma Immunol. Res.* **2021**, *13*, 450–467. [[CrossRef](#)] [[PubMed](#)]
60. Srikakulapu, P.; McNamara, C.A. B Lymphocytes and Adipose Tissue Inflammation. *Arterioscler. Thromb. Vasc. Biol.* **2020**, *40*, 1110–1122. [[CrossRef](#)]
61. Winer, D.A.; Winer, S.; Shen, L.; Wadia, P.P.; Yantha, J.; Paltser, G.; Tsui, H.; Wu, P.; Davidson, M.G.; Alonso, M.N.; et al. B cells promote insulin resistance through modulation of T cells and production of pathogenic IgG antibodies. *Nat. Med.* **2011**, *17*, 610–617. [[CrossRef](#)] [[PubMed](#)]
62. DeFuria, J.; Belkina, A.C.; Jagannathan-Bogdan, M.; Snyder-Cappione, J.; Carr, J.D.; Nersesova, Y.R.; Markham, D.; Strissel, K.J.; Watkins, A.A.; Zhu, M.; et al. B cells promote inflammation in obesity and type 2 diabetes through regulation of T-cell function and an inflammatory cytokine profile. *Proc. Natl. Acad. Sci. USA* **2013**, *110*, 5133–5138. [[CrossRef](#)]
63. Zhou, Z.; Sun, B.; Huang, S.; Jia, W.; Yu, D. The tRNA-associated dysregulation in diabetes mellitus. *Metabolism* **2019**, *94*, 9–17. [[CrossRef](#)]
64. Arroyo, M.N.; Green, J.A.; Cnop, M.; Igoillo-Esteve, M. tRNA Biology in the Pathogenesis of Diabetes: Role of Genetic and Environmental Factors. *Int. J. Mol. Sci.* **2021**, *22*, 496. [[CrossRef](#)] [[PubMed](#)]
65. Antal, Z. Maturity-Onset Diabetes of the Young (MODY): Genetic Causes, Clinical Characteristics, Considerations for Testing, and Treatment Options. *Endocrines* **2021**, *2*, 485–501. [[CrossRef](#)]
66. Jang, K.M. Maturity-onset diabetes of the young: Update and perspectives on diagnosis and treatment. *J. Yeungnam Med. Sci.* **2020**, *37*, 13–21. [[CrossRef](#)]
67. Kant, R.; Davis, A.; Verma, V. Maturity-Onset Diabetes of the Young: Rapid Evidence Review. *Am. Fam. Physician* **2022**, *105*, 162–167.
68. Pirovich, D.B.; Da'dara, A.A.; Skelly, P.J. Multifunctional Fructose 1,6-Bisphosphate Aldolase as a Therapeutic Target. *Front. Mol. Biosci.* **2021**, *8*, 719678. [[CrossRef](#)]
69. Simons, N.; Debray, F.-G.; Schaper, N.C.; Kooi, M.E.; Feskens, E.J.M.; Hollak, C.E.M.; Lindeboom, L.; Koek, G.H.; Bons, J.A.P.; Lefeber, D.J.; et al. Patients With Aldolase B Deficiency Are Characterized by Increased Intrahepatic Triglyceride Content. *J. Clin. Endocrinol. Metab.* **2019**, *104*, 5056–5064. [[CrossRef](#)] [[PubMed](#)]
70. Kim, A.Y.; Hughes, J.J.; Dempsey, A.P.; Schatz, K.S.; Wang, T.; Gunay-Aygun, M. Pitfalls in the Diagnosis of Hereditary Fructose Intolerance. *Pediatrics* **2020**, *146*, e20193324. [[CrossRef](#)] [[PubMed](#)]
71. Li, X.; Wang, F.; Xu, M.; Howles, P.; Tso, P. ApoA-IV improves insulin sensitivity and glucose uptake in mouse adipocytes via PI3K-Akt Signaling. *Sci. Rep.* **2017**, *7*, 41289. [[CrossRef](#)] [[PubMed](#)]
72. von Toerne, C.; Huth, C.; de Las Heras Gala, T.; Kronenberg, F.; Herder, C.; Koenig, W.; Meisinger, C.; Rathmann, W.; Waldenberger, M.; Roden, M.; et al. MASP1, THBS1, GPLD1 and ApoA-IV are novel biomarkers associated with prediabetes: The KORA F4 study. *Diabetologia* **2016**, *59*, 1882–1892. [[CrossRef](#)]
73. Kronenberg, F.; Kuen, E.; Ritz, E.; Konig, P.; Kraatz, G.D.; Lhotta, K.; Mann, J.F.E.; Muller, G.A.; Neyer, U.; Riegel, W.; et al. Apolipoprotein A-IV serum concentrations are elevated in patients with mild and moderate renal failure. *J. Am. Soc. Nephrol. JASN* **2002**, *13*, 461–469. [[CrossRef](#)]
74. Wang, P.-W.; Hung, Y.-C.; Wu, T.-H.; Chen, M.-H.; Yeh, C.-T.; Pan, T.-L. Proteome-based identification of apolipoprotein A-IV as an early diagnostic biomarker in liver fibrosis. *Oncotarget* **2017**, *8*, 88951–88964. [[CrossRef](#)]
75. Qu, J.; Fourman, S.; Fitzgerald, M.; Liu, M.; Nair, S.; Oses-Prieto, J.; Burlingame, A.; Morris, J.H.; Davidson, W.S.; Tso, P.; et al. Low-density lipoprotein receptor-related protein 1 (LRP1) is a novel receptor for apolipoprotein A4 (APOA4) in adipose tissue. *Sci. Rep.* **2021**, *11*, 13289. [[CrossRef](#)]
76. Karagiannides, I.; Abdou, R.; Tzortzopoulou, A.; Voshol, P.J.; Kypreos, K.E. Apolipoprotein E predisposes to obesity and related metabolic dysfunctions in mice. *FEBS J.* **2008**, *275*, 4796–4809. [[CrossRef](#)]



77. Kypreos, K.E.; Karagiannides, I.; Fotiadou, E.H.; Karavia, E.A.; Brinkmeier, M.S.; Giakoumi, S.M.; Tsompanidi, E.M. Mechanisms of obesity and related pathologies: Role of apolipoprotein E in the development of obesity. *FEBS J.* **2009**, *276*, 5720–5728. [[CrossRef](#)]
78. Zhao, Z.; Zou, S.; Guan, X.; Wang, M.; Jiang, Z.; Liu, Z.; Li, C.; Lin, H.; Liu, X.; Yang, R.; et al. Apolipoprotein E Overexpression Is Associated With Tumor Progression and Poor Survival in Colorectal Cancer. *Front. Genet.* **2018**, *9*, 650. [[CrossRef](#)]
79. Chen, Y.-C.; Pohl, G.; Wang, T.-L.; Morin, P.J.; Risberg, B.; Kristensen, G.B.; Yu, A.; Davidson, B.; Shih, I.-M. Apolipoprotein E is required for cell proliferation and survival in ovarian cancer. *Cancer Res.* **2005**, *65*, 331–337. [[CrossRef](#)] [[PubMed](#)]
80. Shintaku, H. Disorders of tetrahydrobiopterin metabolism and their treatment. *Curr. Drug Metab.* **2002**, *3*, 123–131. [[CrossRef](#)] [[PubMed](#)]
81. Citron, B.A.; Kaufman, S.; Milstien, S.; Naylor, E.W.; Greene, C.L.; Davis, M.D. Mutation in the 4a-carbinolamine dehydratase gene leads to mild hyperphenylalaninemia with defective cofactor metabolism. *Am. J. Hum. Genet.* **1993**, *53*, 768–774. [[PubMed](#)]
82. Bolus, W.R.; Kennedy, A.J.; Hasty, A.H. Obesity-induced reduction of adipose eosinophils is reversed with low-calorie dietary intervention. *Physiol. Rep.* **2018**, *6*, e13919. [[CrossRef](#)] [[PubMed](#)]
83. Calco, G.N.; Fryer, A.D.; Nie, Z. Unraveling the connection between eosinophils and obesity. *J. Leukoc. Biol.* **2020**, *108*, 123–128. [[CrossRef](#)]
84. Al-Jamal, H.A.N.; Johan, M.F.; Jusoh, S.A.M.; Ismail, I.; Taib, W.R.W. Re-Expression of Bone Marrow Proteoglycan-2 by 5-Azacytidine is associated with STAT3 Inactivation and Sensitivity Response to Imatinib in Resistant CML Cells. *Asian Pac. J. Cancer Prev.* **2018**, *19*, 1585–1590.
85. Wang, Y.; Li, X.; Cao, Y.; Xiao, C.; Liu, Y.; Jin, H. Effect of the ACAA1 Gene on Preadipocyte Differentiation in Sheep. *Front. Genet.* **2021**, *12*, 649140. [[CrossRef](#)]
86. Deng, T.; Wu, J.; Abdel-Shafy, H.; Wang, X.; Lv, H.; Shaukat, A.; Zhou, X.; Zhou, Y.; Sun, H.; Wei, P.; et al. Comparative Genomic Analysis of the Thiolase Family and Functional Characterization of the Acetyl-Coenzyme A Acyltransferase-1 Gene for Milk Biosynthesis and Production of Buffalo and Cattle. *J. Agric. Food Chem.* **2023**, *71*, 3325–3337. [[CrossRef](#)]
87. Howell, K.R.; Powell, T.L. Effects of maternal obesity on placental function and fetal development. *Reproduction* **2017**, *153*, R97–R108. [[CrossRef](#)]
88. Samuelsson, A.M.; Matthews, P.A.; Argenton, M.; Christie, M.R.; McConnell, J.M.; Jansen, E.H.; Piersma, A.H.; Ozanne, S.E.; Twinn, D.F.; Remacle, C.; et al. Diet-induced obesity in female mice leads to offspring hyperphagia, adiposity, hypertension, and insulin resistance: A novel murine model of developmental programming. *Hypertension* **2008**, *51*, 383–392. [[CrossRef](#)]

**Disclaimer/Publisher’s Note:** The statements, opinions and data contained in all publications are solely those of the individual author(s) and contributor(s) and not of MDPI and/or the editor(s). MDPI and/or the editor(s) disclaim responsibility for any injury to people or property resulting from any ideas, methods, instructions or products referred to in the content.